Simulating Bell inequality violations with classical optics encoded qubits

Matias A. Goldin, Diego Francisco,* and Silvia Ledesma

Departamento de Física, Facultad de Ciencias Exactas y Naturales, Universidad de Buenos Aires, Ciudad Universitaria, 1428 Buenos Aires, Argentina
**Corresponding author: dfrancis@df.uba.ar*

Received August 13, 2009; revised December 30, 2009; accepted January 11, 2010;
posted February 12, 2010 (Doc. ID 115711); published March 31, 2010

We present here a classical optics device based on an imaging architecture as an analogy of a quantum system where the violation of the Bell inequality can be evidenced. Quantum states are encoded using an electromagnetic wave modulated in amplitude and phase. Unitary operations involved in the measurement of the observables are simulated with the use of a coherent optical processor. The images obtained in the output of the process contain all the information about the possible outcomes of the joint measurement. By measuring the intensity distribution in the image plane we evaluate the mean values of the simulated observables. The obtained experimental results show how some correlations of Clauser–Horne–Shimony–Holt-type exceed the upper bound imposed by the local realism hypothesis as a consequence of the joint effect of entanglement and two-particle interference.

OCIS codes: 000.1600, 200.3050, 270.5585.

1. INTRODUCTION

In this paper we present a classical wave optics analogy of some well known quantum experiments involving Bell inequality violations. The optical simulation of quantum systems is based on the wave features of quantum mechanics. The main idea is to exploit the wave nature of the electromagnetic field in order to represent the quantum state of one or more particles. In this representation, the probability amplitude of the occurrence of each state of a basis is associated with the complex amplitude of the electromagnetic field, and temporal evolutions are simulated by means of the propagation of the field through an optical system. Quantum phenomena can be understood as a consequence of the wave nature of the evolution of quantum states. In this sense, the wave character of the electromagnetic field allows us to simulate, in a pictorial way, the behavior of the quantum world that usually contradicts common sense. Moreover, the classical electromagnetic field works as an ontological representation of the wave function and it is a useful tool to visualize the structure of problems that are usually complex and counterintuitive. This kind of analogy between quantum mechanics and optics has been explored in different ways. In pioneer works, polarizations and paths of single photons [1] or classical electromagnetic waves [2,3] were used for encoding qubits. In several later works, qubits were encoded in the spatial modulation of the transverse amplitude of an electromagnetic field [4–8], in the transverse modes of the optical field propagating in multimode waveguides [9], or in the polarization of two classical fields with different frequencies [10]. In all cited works it was proven that, in addition to potential applications, the study of this kind of simulations of quantum systems may help one to elucidate the fundamental differences between classical wave and quantum systems. Particularly, the exploration of classical wave analogies of quantum nonlocality is interesting not only from an academic point of view but also to yield new insights into fundamental features of quantum mechanics.

Violation tests of Bell inequalities have become a fundamental tool for experimentally proving the presence of entanglement correlations in quantum systems of general interest in areas of quantum information, quantum computation, and foundations of quantum mechanics. In a seminal paper [11] Einstein, Podolsky, and Rosen (EPR) established their argument of the so-called local realism hypothesis. According to it, if we accept that certain properties of a measured system are present prior to and independent of the observation, then quantum mechanics is not a complete theory of nature. Almost 20 years later, Bell [12] showed that, for systems composed of two spin 1/2 particles, measurements of some correlated quantities should yield different results in the quantum mechanical case to those expected if we accept the local realism criterion of EPR. Many experiments confirmed the quantum predictions using Bell-like systems as entangled photons in polarization degrees of freedom [13–20], entangled photons in position-momentum degrees of freedom [21], and entangled atoms [22]. More recently, a novel simulation of Bell inequality violations using nuclear magnetic resonance (NMR) techniques was reported [23]. In [24] we can find a complete review on Bell inequality violations and related problems as hidden variable theories.

In this paper we will show a classical optics analogy of Bell inequality violations. It can be simulated using an imaging architecture similar to those used in optical processing. In our scheme, qubits are represented as images and unitary evolution is simulated by means of coherent optical processors. The paper is organized as follows: in Section 2 we give a brief review of the basic general con-

cepts of Bell inequality violations. In Sections 3 and 4 we present some considerations about optical simulations of quantum information processing by means of imaging architectures. In Section 5, we present the optical setup for the particular case of the simulation of the Bell inequality violations. In Section 6 we present experimental results. Finally we summarize our conclusions in Section 7.

2. BELL INEQUALITIES

We will use in this paper the following notation: a state of the two-dimensional Hilbert space (or the qubit space) is denoted as a complex linear combination of the two states of the computational basis $\{|0\rangle,|1\rangle\}$. A separable state of the 2^2-dimensional space of a composed system of two qubits is denoted as the product $|\Psi(A)\rangle_A \otimes |\Psi(B)\rangle_B$, where $|\Psi(j)\rangle_j = \alpha_j|0\rangle_j + \beta_j|1\rangle_j$ (with $j=A,B$) is the quantum state associated with the qubit A or B, respectively. In what follows we briefly describe the Clauser–Horne–Shimony–Holt (CHSH) approach to Bell-type experiments [25]. Let us suppose that two spacelike separated observers (Alice and Bob) share an ensemble of entangled states $|\Psi\rangle_{AB} = (|0\rangle_A \otimes |0\rangle_B + |1\rangle_A \otimes |1\rangle_B)/\sqrt{2}$ (subindices A and B denote the observers or, equivalently, the qubits they will each measure). Let us consider two pairs of local physical observables: A and A' for Alice, and B and B' for Bob. As usual, we will define these observables as

$$A = \hat{\alpha}\cdot\vec{\sigma}_A, \quad A' = \hat{\alpha}'\cdot\vec{\sigma}_A, \quad B = \hat{\beta}\cdot\vec{\sigma}_B, \quad B' = \hat{\beta}'\cdot\vec{\sigma}_B, \tag{1}$$

where $\hat{\alpha},\hat{\alpha}',\hat{\beta},\hat{\beta}'$ are unit vectors and $\vec{\sigma}_A$ and $\vec{\sigma}_B$ are vectors whose components are the Pauli matrices operating on the local subspaces associated with Alice and Bob, respectively.

If Alice and Bob make a random choice of one observable of their pair and then perform a simultaneous measurement, they have the following four possible nonlocal combinations: $A\otimes B$, $A\otimes B'$, $A'\otimes B$, and $A'\otimes B'$. After several repetitions of the experiment, they can calculate the expected value of the quantity $O = A\otimes B + A\otimes B' + A'\otimes B' - A'\otimes B$. Since Pauli matrices do not commute, quantum mechanics asserts that the four nonlocal observables in each term of O are not compatible and therefore cannot be simultaneously measured. Moreover, the Bohr principle of complementarity [26] claims that we are forbidden to consider simultaneously the possible outcomes of mutually exclusive experiments. However, according to the local realism hypothesis, there exist local hidden parameters which completely determine the outcomes of the chosen measurement. Moreover, these parameters also determine the outcomes that we would have if we have measured an observable which is incompatible with that actually measured. We have no control on hidden parameters and so there are some degrees of freedom that are not precisely known. In the case of the Bell experiment, each hidden parameter assigns well defined outcomes of ± 1 to each local measurement. It has been demonstrated that under such a condition the expected value of the nonlocal quantity O satisfies the CHSH form of the Bell inequality [25],

$$|\langle O\rangle| = |\langle A\otimes B\rangle + \langle A\otimes B'\rangle + \langle A'\otimes B'\rangle - \langle A'\otimes B\rangle| \le 2. \tag{2}$$

We will inspect the particular case $\widehat{\alpha'} = \widehat{\beta'} = \hat{z}$ so that $A' = B' \equiv C$. With this assumption, $\langle A'\otimes B'\rangle = \langle C\otimes C\rangle = \hat{z}\cdot\hat{z} = +1$ for the state we have chosen, and the left of the Bell inequality (2) becomes

$$\langle O\rangle = \langle A\otimes B\rangle + \langle A\otimes C\rangle - \langle C\otimes B\rangle \le 1. \tag{3}$$

The equation above must be satisfied for arbitrarily chosen observables A and B with $C=\sigma_z$. Without loss of generality and for practical reasons, we will set the following three observables:

$$A = \sigma_x, \quad B = \sin\theta\,\sigma_x + \cos\theta\,\sigma_z, \quad C = \sigma_z. \tag{4}$$

Additionally, in order to emphasize the role of two-particle interference effects in the mechanism of Bell inequality violations, we will analyze both the case of maximally entangled states and the case of mixed states. Let us consider the expectation value of the quantity O with respect to the mixed state whose density matrix is the convex sum of the pure entangled state $\rho_{\text{pure}} = |\Psi\rangle_{AB}\langle\Psi|_{AB}$ and the maximally mixed state: $\rho_{\text{mixed}} = \frac{1}{2}[(|0\rangle_A \otimes |0\rangle_B)(\langle 0|_A \otimes \langle 0|_B) + (|1\rangle_A \otimes |1\rangle_B)(\langle 1|_A \otimes \langle 1|_B)]$. Therefore the state can be written as

$$\rho = q\rho_{\text{pure}} + (1-q)\rho_{\text{mixed}} = \frac{1}{2}\begin{pmatrix} 1 & 0 & 0 & q \\ 0 & 0 & 0 & 0 \\ 0 & 0 & 0 & 0 \\ q & 0 & 0 & 1 \end{pmatrix}, \tag{5}$$

where the matrix representation is given in the computational basis $\{|0\rangle_A,|1\rangle_A\}\otimes\{|0\rangle_B,|1\rangle_B\}$ and $q\in[0,1]$. The state of Eq. (5) is a pure state for $q=1$ and becomes mixed if $0\le q<1$ owing to the loss of the off-diagonal coherence components of the density matrix. The maximally mixed state corresponds to $q=0$. Evaluating the expected value of the quantity O with respect to state (5) and setting the observables defined in Eq. (4) we have

$$\begin{aligned}\langle O(\theta)\rangle &= \mathrm{tr}[(A\otimes B)\rho] + \mathrm{tr}[(A\otimes C)\rho] - \mathrm{tr}[(C\otimes B)\rho] \\ &= q\sin\theta - \cos\theta.\end{aligned} \tag{6}$$

This last result contradicts the Bell inequality (3) if $\theta_c(q) < \theta < \pi$, where $\theta_c(q)$ is the solution of the equation $q = (1+\cos\theta)/\sin\theta$ that always exists in the interval $0<\theta<\pi$ for all $0<q\le 1$. The maximal violation occurs for $q=1$ and corresponds to the Bell state which is pure and maximally entangled. On the contrary, there is no quantum correlations in the case of the maximally mixed state $q=0$ and therefore the Bell inequality is not violated. In the next sections we will describe the problem underlined above with elements of classical optics.

3. ENCODING QUBITS IN OPTICAL SCENES

We use a method which is extensively discussed in the literature [2,3,5] based on the representation of qubits as position C-bits. According to this method in the input scene we encode the logical values $|0\rangle$ and $|1\rangle$ of a single qubit in two slices located in the left and right halves of

the full plane, respectively. Let (x_o, y_o) be the coordinates of the input plane. As the representation is one-dimensional, we have translational symmetry with respect to the y_o axis, and we can consider only the x_o coordinate. According to the wave function formalism, the optical analogy suggests the following notation:

$$\langle x_o|0\rangle \equiv \mathrm{Rect}\left(\frac{x_o + a}{b}\right), \quad \langle x_o|x_o\rangle \equiv \mathrm{Rect}\left(\frac{x_o - a}{b}\right), \quad (7)$$

where $\mathrm{Rect}(x)$ is a unit rectangle function that takes the values of 1 if $|x| \leq 1/2$ and 0 in the other case. Equation (7) describes unit amplitude transmittance in a rectangle of width b centered at $x = \pm a$ $(b \ll a)$ where the computational state $|0\rangle$ is associated with the left rectangle and the computational state $|1\rangle$ is associated with the right rectangle as it is shown in Fig. 1(a). To encode the more general state of two qubits, the modulation of the complex amplitude of the field in both slices is needed as we can see in Fig. 1(b). The optical analogy of the quantum measurement process is very simple. In fact, if the state $|\varphi\rangle = \alpha|0\rangle + \beta|1\rangle$ is represented, the relative intensities of the slices will be precisely $|\alpha|^2$ and $|\beta|^2$ and, after renormalization $|\alpha|^2 + |\beta|^2 = 1$, they can be interpreted as the probabilities associated with the measurement outcomes of $+1$ and -1 in a projective measurement in the computational basis. A quantum measurement is equivalent to keeping the left slice with probability $|\alpha|^2$ or the right slice with probability $|\beta|^2$. Moreover, the expected value of σ_z on the state represented can be calculated by extracting information from the image presented in Fig. 1(b) as $\langle \sigma_z \rangle = \mathrm{tr}(\sigma_z|\varphi\rangle\langle\varphi|) = (|\alpha|^2 - |\beta|^2)/(|\alpha|^2 + |\beta|^2)$. The scheme described above is easily generalizable to represent two or more qubits. We can see in Fig. 2 the convention we will use to accomplish this. We denote A as the qubit encoded in the up-down direction and B as the qubit encoded in the left-right direction. In this case the representation of the two qubit basis will be a two-dimensional extension of Eq. (7).

A. Pure and Mixed States: The Optical Approach

We will briefly introduce here how we can extend our simulation to the case of mixed states. A mixed state with density matrix $\rho = \Sigma_i p_i |\varphi_i\rangle\langle\varphi_i|$, where $p_i \geq 0$ and $\Sigma_i p_i = 1$, consists of a set of pure states $\{|\varphi_i\rangle, i = 1, 2, \ldots, n\}$, each appearing with its respective probability p_i. The strategy we use to simulate and measure mixed states is as follows: first we represent an image in the input plane that simulates the member of the ensemble $|\varphi_i\rangle$, which is a pure state. Then we calculate the expected value of σ_z, $\langle \sigma_z \rangle$, as we have discussed in Section 3, then we multiply the result by p_i, and finally we sum up all the results. In this way, since $\mathrm{tr}(\sigma_z \rho) = \Sigma_i p_i \, \mathrm{tr}(\sigma_z|\varphi_i\rangle\langle\varphi_i|)$ the same values as having a statistical ensemble will be obtained. It is worth mentioning that following this procedure another analogy can be achieved using a temporal succession of images with a duration T_i. If the total time of the experiment is T, then we select the times so that $T_i/T = p_i$. In this case, one has to integrate the output images in the time T of the experiment. This could be realized using an optical element capable of modulating the light field in the input plane in a dynamical way. For practical reasons, we used the first strategy throughout our work.

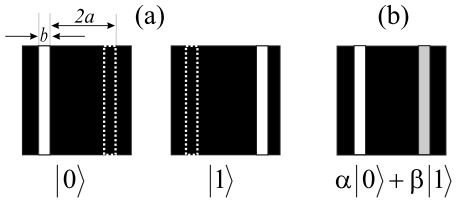

Fig. 1. Optical representation of the single qubit state. (a) Optical representation of the states of the computational basis. (b) The input scene associated with the optical single qubit. The state $\alpha|0\rangle + \beta|1\rangle$ is represented by the "left" or "right" slices where the constants α and β are the complex amplitudes of the electromagnetic field in each slice.

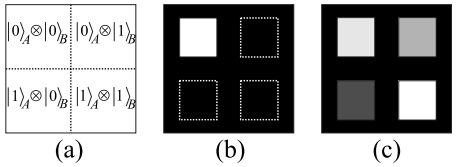

Fig. 2. Schematic picture of the representation of two qubit states by using optical scenes. (a) Spatial organization of the input plane in order to emulate two qubit states. (b) Optical representation of the $|0\rangle_A \otimes |0\rangle_B$ state. (c) Optical representation of the general pure two qubit state. Gray level scale corresponds to different amplitudes and phase modulations of the classical wavefront.

4. THE OPTICAL $U(2)$ OPERATOR

The key of our work is the possibility of simulating unitary operations acting on a single qubit space. In what follows we denote the field amplitude as depending on a single relevant coordinate due to the one-dimensional character of the optical simulation of local U(2) operators. The simulation of U(2) operators acting on single qubit states works as follows. The quantum state is encoded in an input scene located in the previous focal plane of a spherical lens of focal distance f. For collimated illumination, this lens allows one to obtain on its back focal plane the Fourier transform of the input scene, which corresponds to a field distribution whose relevant coordinate is x_F. The relationship between the spatial frequency variable f_x and the position coordinate x_F on the Fourier plane is $f_x = x_F/\lambda f$, where λ is the wavelength of the light field. In the Fourier plane, a spatial filter of complex transmittance $H(f_x)$ is placed. A second spherical lens of focal distance f is placed so that its previous focal plane lies in the Fourier plane. This lens allows one to obtain the inverse Fourier transform of the product between the Fourier transform of the input transmittance and the function $H(f_x)$. The field amplitude in the output plane is the convolution between the input complex amplitude and the so-called impulse response of the system that is defined as the inverse Fourier transform of the function $H(f_x)$ [27]. In our case, spatial filtering in the Fourier plane is performed by an almenary phase grating which is a square wave phase modulation of amplitude $0 < \phi < 2\pi$ and spatial period $2p$. We denote the width of each square pulse as p and the position of the center of the pulse in the frequency domain as f_c. The complex transmittance of the filter is

$$H(f_x) = \begin{cases} e^{i\phi}, & \text{if } |f_x - f_c| < p/2 \\ 1, & \text{in other case,} \end{cases} \tag{8}$$

where the function above is defined in $f_x \in [-p, p]$ and is extended by periodicity for all $f_x \in \Re$. The complex transmittance defined in Eq. (8) could be expanded in terms of pure harmonic components so that the function $H(f_x)$ is written as $H(f_x) = \Sigma_{n \in Z} C_n \exp(i(\pi n/p) f_x)$. Taking into account only the three central diffracted orders (coefficients C_0 and $C_{\pm 1}$), the inverse Fourier transform of the equation above is

$$\begin{aligned} h(x) &= \int_{-\infty}^{+\infty} H(f_x) \exp(i 2\pi f_x x) df_x \\ &= \cos\frac{\phi}{2}\delta(x) + \frac{2}{\pi}\sin\frac{\phi}{2}e^{i\gamma^-}\delta\left(x + \frac{1}{2p}\right) \\ &\quad + \frac{2}{\pi}\sin\frac{\phi}{2}e^{i\gamma^+}\delta\left(x - \frac{1}{2p}\right), \end{aligned} \tag{9}$$

where we have defined the phase constants $\gamma^{\pm} = \pi/2 \pm (\pi/p) f_c$. Let us suppose now that in the input scene we represent a complex linear combination of the two computational states $\langle x_o|\Psi_{\text{in}}\rangle = \alpha\langle x_o|0\rangle + \beta\langle x_o|1\rangle$ according to Eq. (7). The output signal $\langle x_i|\Psi_{\text{out}}\rangle$ will be equal to $(h * \Psi_{\text{in}})_{(x_i)}$ corresponding to the convolution between the input signal and the impulse response of the system defined in Eq. (9) evaluated in the coordinate x_i of the image plane. The result gives six terms that are the three principal diffracted orders of the two slices that represent the computational states. Under certain conditions that can be experimentally controlled, the expression can be simplified. In fact, if we choose a grating whose spatial frequency satisfies the relationship $2p = 1/2a$ with respect to the spatial separation $2a$ of the slices, the separation of the diffracted orders in the final plane will be equal to the distance of the two slices, allowing the interference between them as it is suggested in Fig. 3. All diffracted orders located out of the computational regions are not registered.

The input-output relation of the process in matrix form, using the identifications of Eq. (7) is expressed in the representation of the computational basis as

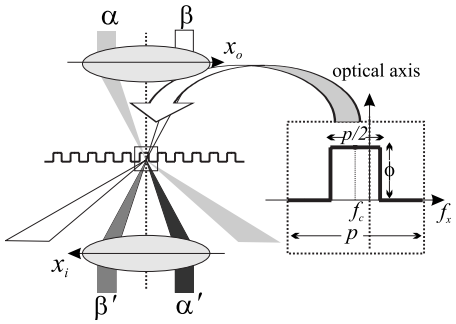

Fig. 3. Schematic picture of the optically simulated U(2) operation. Complex amplitudes α and β are mapping onto α' and β' by means of a $4f$ coherent optical processor with an almenary phase grating in the Fourier plane.

$$\begin{pmatrix} \alpha \\ \beta \end{pmatrix} \to \begin{pmatrix} \alpha' \\ \beta' \end{pmatrix} = \begin{pmatrix} \cos\frac{\phi}{2} & \frac{2}{\pi}\sin\frac{\phi}{2}e^{i\gamma^-} \\ \frac{2}{\pi}\sin\frac{\phi}{2}e^{i\gamma^+} & \cos\frac{\phi}{2} \end{pmatrix} \begin{pmatrix} \alpha \\ \beta \end{pmatrix}, \tag{10}$$

where ϕ and $\gamma^{\pm}$ are real-valued. The process is schematized in Fig. 3. The similarity between the general expressions of U(2) operators and the two-parameter family of linear operators of Eq. (10) becomes evident. For instance, if we want to measure the observable σ_x, we must apply the Hadamard operator H [28] and then perform the measurement in the computational basis. This can be done by setting $\tan(\phi/2) = 2/\pi$ and $f_c = -p/2$. The Hadamard-like operator $\sqrt{2}H\sigma_z$ obtained in this way can be transformed in the proper Hadamard operator by placing a phase plate σ_z in the front of the first lens since $\sigma_i^2 = 1 \forall i$ after renormalization. Measurement of Hermitian observables defined in the Hilbert space of the two level quantum system can be simulated in the same way. In Table 1 we show the unitary change of basis associated with each observable of Eq. (4) and the corresponding values of the parameters ϕ and f_c. A phase shift σ_z in front of the first lens must be eventually included.

5. OPTICAL IMPLEMENTATION OF THE ANALOGY

The experiment reported in this section, works as a classical optics analogy of the Bell experiment. We will test our setup in two cases which correspond to the two states $q = 1$ and 0 described in Eq. (5). In the first case ($q = 1$) Alice and Bob will share an entangled pair. For simulating this, we encode the maximally entangled state $|\Psi\rangle_{AB} = (|0\rangle_A \otimes |0\rangle_B + |1\rangle_A \otimes |1\rangle_B)/\sqrt{2}$ by uniform illumination of the top-left *and* the down-right quarters of the full input plane [Fig. 4(a)]. In the second case ($q = 0$) the input state will be the statistical mixture represented by the density matrix $\rho_{\text{mixed}} = \frac{1}{2}[(|0\rangle_A \otimes |0\rangle_B)(\langle 0|_A \otimes \langle 0|_B) + (|1\rangle_A \otimes |1\rangle_B)(\langle 1|_A \otimes \langle 1|_B)]$ whose optical analogy is the uniform illumination of the top-left *or* the down-right quarters of the full input plane, each with a probability of 1/2. This is an incoherent superposition of the computational states and it should not have any quantum correlation [Fig. 4(b)].

The complete optical setup is schematized in Fig. 5. An argon laser source ($\lambda = 477$ nm) is filtered and then collimated with lens L_0. The collimated beam impinges onto the binary mask P_i which represents the two qubit state that Alice and Bob use during the experiment. The input scene is placed in the previous focal plane of the lens L_1 (focal length of 26 cm) that allows one to obtain the Fourier transform of the input in its back focal plane or Fou-

Table 1. Hermitian Observables, Unitary Change of Basis, and Parameters of the Optical Simulation

Hermitian	Unitary	ϕ	f_c	Phase
σ_x	H	$2\arctan(2/\pi)$	$-p/2$	σ_z
$\sin\theta\,\sigma_x + \cos\theta\,\sigma_z$	$e^{-i\theta\sigma_y/2}\sigma_z$	$2\arctan((2/\pi)\tan(\theta/2))$	$-p/2$	σ_z
σ_z	1	—	—	—

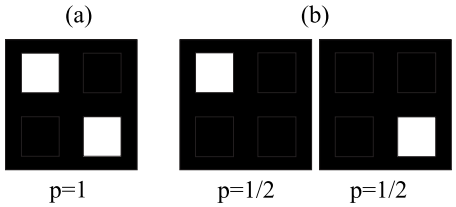

Fig. 4. Optical representation (a) of the maximally entangled state, $(|0\rangle_A \otimes |0\rangle_B + |1\rangle_A \otimes |1\rangle_B)/\sqrt{2}$, and (b) of the maximally mixed state, $\frac{1}{2}[(|0\rangle_A \otimes |0\rangle_B)(\langle 0|_A \otimes \langle 0|_B) + (|1\rangle_A \otimes |1\rangle_B)(\langle 1|_A \otimes \langle 1|_B)]$, as optical scenes.

rier plane. In the Fourier plane, we place the spatial filter for simulating two local unitary operators. According to previous discussions, this can be done with the composition of two orthogonal almenary phase gratings as shown in Fig. 6. Horizontal phase grating with phase modulation parameter ϕ_A produces diffracted orders in the "up-down" direction from where Alice's qubit is encoded. Vertical phase grating with parameter ϕ_B produces diffracted orders in the "left-right" direction associated with Bob's subsystem. The two-dimensional almenary phase grating, whose phase modulation goes from 0 to $\phi_A + \phi_B$ (mod 2π) was programmed in a spatial light modulator (SLM). This device consists of a Sony liquid crystal display television (LCTV) that combined with two polarizers (P_1 and P_2) and two quarter wave plates (QWP_1 and QWP_2) acts as a mostly phase modulator [29]. The LCTV (model LCX012BL) was extracted from a commercial video-projector and is a video graphics array (VGA) resolution panel (640 × 480 pixels) with square pixels of 34 μm size separated by a distance of 41.3 μm. The process is completed with the lens L_2 (focal length of 26 cm) that allows one to obtain the inverse Fourier transform. The final image in the output plane P_o is captured by a video camera [charge-coupled device (CCD)]. The video camera is a Sony CCD model "Iris, Black and White" 640 × 480 pixels.

According to Table 1, an additional phase plate that introduces a π phase shift in the left-bottom and in the right-top quarters of the input wavefront must be included. Therefore, this phase plate does not affect the illuminated zone of the input plane and we can ignore it. Moreover, in the final image, we must take into account the inversion of the coordinates system whose senses are indicated with arrows on the P_i and P_o input and output planes, respectively, in Fig. 5. The protocol of the full experiment is depicted in Fig. 6 and can be described as follows: each local operation is simulated by using one of the two orthogonal almenary phase gratings. The horizontal modulation from 0 to ϕ_A simulates unitary operations on the Alice up-down encoded qubit, while the vertical modulation from 0 to ϕ_B works equally for the Bob left-right encoded qubit (Fig. 7). The Alice measurement is fixed to σ_x (or σ_z) and, therefore, eventually she only applies a Hadamard operator before projecting her qubit on the computational basis. The Bob measurement is varying as $\sin\theta\,\sigma_x + \cos\theta\,\sigma_z$ for $0 \le \theta \le 2\pi$ and the phase modulation $\phi_B(\theta) = 2\arctan((2/\pi)\tan(\theta/2))$ (see Table 1) has to be variable. In both cases the amplitude of the phase modulation is controlled directly by the SLM. Measurement of σ_z is performed by orthogonal projection on the computational basis and no phase modulation is needed. The output scenes corresponding to the three pairs of local measurements (one fixed $A \otimes C$ and two varying $A \otimes B$ and $C \otimes B$) are registered by the CCD and recorded for its posterior analysis. The analysis method and the corresponding results will be shown in the next section.

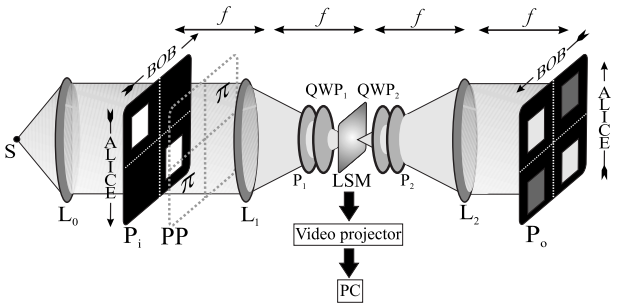

Fig. 5. Experimental setup for simulating the Bell experiment as an imaging system.

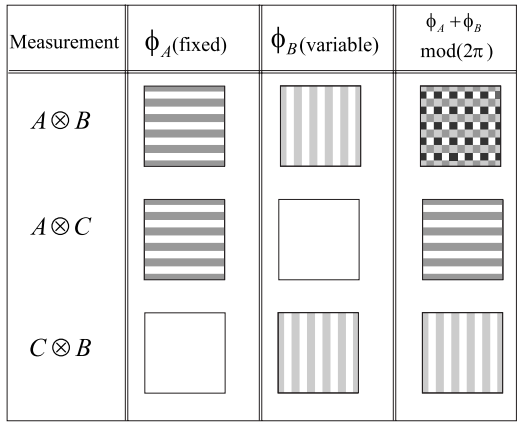

Fig. 6. Detail of the protocol of the full experiment.

6. BELL INEQUALITIES: EXPERIMENTAL RESULTS

Once the output scenes corresponding to each measurement are obtained, the mean value of the observable $\langle O \rangle$ can be easily evaluated. Unitary changes of basis reduce

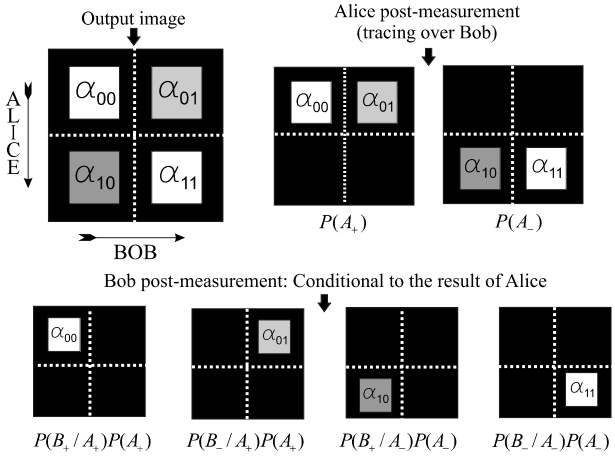

Fig. 7. Measuring a two qubit system in computational basis from the output distribution intensities.

the problem of the measurement of an arbitrary observable into the problem of measuring $\sigma_z \otimes \sigma_z$. This is a projective measurement in the computational basis $\{|0\rangle_A, |1\rangle_A\} \otimes \{|0\rangle_B, |1\rangle_B\}$. The results of a projective measurement in the computational basis can be easily interpreted in terms of the distributed intensities of the output field obtained in our experiment. The underlying process in the analysis of the output images is depicted in Fig. 7. In what follows $P(A_i, B_j)$ with $i, j = \pm 1$ is the joint probability of, after a projective measurement in computational basis, $A = i$ and $B = j$, i.e., the measurement outcomes obtained by Alice and Bob were i and j, respectively. According to the elementary probability theory, this quantity can be evaluated as $P(A_i, B_j) = P(B_j/A_i)P(A_i)$, where $P(B_j/A_i)$ is the conditional probability of $B = j$ knowing that the result $A = i$ was obtained, and $P(A_i)$ is the probability that the result $A = i$ was obtained, independent of Bob.

Let us suppose that Alice performs the measurement of her qubit. As we have discussed above, it means that she has to keep the up or the down half of the full plane with different probabilities. The statistical properties of Alice's measurement are described by the marginal probabilities deduced from the joint distribution integrated over the degree of freedom associated with Bob. In the formalism of quantum mechanics, the marginal distribution of Alice is defined by the reduced density matrix $\mathrm{tr}_B(\rho_{AB})$. From the optical point of view, the partial trace over Bob's subsystem means that the accessible information available for Alice is related to the field distribution in the up-down direction, independent to the field distribution in the left-right direction from where the information available for Bob is encoded. So, the two possible post-measurement states of the full system with their respective probabilities will be $|0\rangle_A \otimes (\alpha_{00}|0\rangle_B + \alpha_{01}|1\rangle_B)/\sqrt{|\alpha_{00}|^2 + |\alpha_{01}|^2}$ with probability $P(A_+) = (|\alpha_{00}|^2 + |\alpha_{01}|^2)/(|\alpha_{00}|^2 + |\alpha_{01}|^2 + |\alpha_{10}|^2 + |\alpha_{11}|^2)$, which means that Alice measurement outcome was +1 and her pseudorandom choice was the top half of the scene, or $|1\rangle_A \otimes (\alpha_{10}|0\rangle_B + \alpha_{11}|1\rangle_B)/\sqrt{|\alpha_{10}|^2 + |\alpha_{11}|^2}$ with probability $P(A_-) = (|\alpha_{10}|^2 + |\alpha_{11}|^2)/(|\alpha_{00}|^2 + |\alpha_{01}|^2 + |\alpha_{10}|^2 + |\alpha_{11}|^2)$, which means that the outcome was -1 and her choice was the bottom half of the scene.

Now is Bob's turn. The post-measurement state of the full system after the Bob measurement will be conditioned for the result previously obtained by Alice. The four possible post-measurement states are naturally the four computational states. For instance, the post-measurement state $|0\rangle_A \otimes |0\rangle_B$ can be obtained with probability $P(B_+/A_+) = |\alpha_{00}|^2/(|\alpha_{00}|^2 + |\alpha_{01}|^2)$ with the previous knowledge that the post-measurement state obtained by Alice was $|0\rangle_A \otimes (\alpha_{00}|0\rangle_B + \alpha_{01}|1\rangle_B)/\sqrt{|\alpha_{00}|^2 + |\alpha_{01}|^2}$. At this point the nonlocal aspects of the joint measurement become evident. In this last case, the full process is a joint projective measurement of the output state in the computational basis from where the result $A = +1$, $B = +1$ is obtained. The corresponding post-measurement state will be $|0\rangle_A \otimes |0\rangle_B$ with probability $P(A_+, B_+) = P(B_+/A_+)P(A_+) = |\alpha_{00}|^2/(|\alpha_{00}|^2 + |\alpha_{01}|^2 + |\alpha_{10}|^2 + |\alpha_{11}|^2)$. The remaining three computational states can be equally obtained as post-measurement states with probabilities depending on the intensity distribution $|\alpha_{mn}|^2$, with $m, n = 0, 1$. Therefore, the expected value of $\sigma_z \otimes \sigma_z$ in terms of the output intensity distribution is

$$\langle \sigma_z \otimes \sigma_z \rangle = P(A_+, B_+) + P(A_-, B_-) - P(A_+, B_-) - P(A_-, B_+) = \frac{|\alpha_{00}|^2 + |\alpha_{11}|^2 - |\alpha_{01}|^2 - |\alpha_{10}|^2}{|\alpha_{00}|^2 + |\alpha_{01}|^2 + |\alpha_{10}|^2 + |\alpha_{11}|^2}. \quad (11)$$

It should be pointed out that the Alice and Bob measurements involve only local operations. So the result of the previous analysis does not depend on the chronological order of the measurements since local operators commute with each other. This is important since Alice and Bob measure simultaneously according to the EPR locality hypothesis.

Calculations involved in Eq. (11) are performed directly from the relative output intensities associated with the computational states in the output image. The experiment consists of performing a sampling on the phase modulation of the vertical grating with $0 \le \phi_B < 2\pi$ and, for each value of ϕ_B, evaluating the quantity $\langle O \rangle = \langle A \otimes B \rangle + \langle A \otimes C \rangle - \langle C \otimes B \rangle$ in the function of $\theta = 2 \arctan((\pi/2)\tan(\phi_B/2))$ by inspecting the output images. The experimental results for $\langle O \rangle$ versus θ are plotted together with the theoretical expected result $q \sin\theta - \cos\theta$. Theoretical and experimental curves are compared with 1 in order to explore possible violations of the inequality $q \sin\theta - \cos\theta \le 1$. Experimental results are summarized in Fig. 8.

In Fig. 8(a) $\langle O \rangle$ versus θ is plotted in the full range $\theta \in [0, 2\pi)$ for the maximally entangled state $q = 1$ and for the mixed state $q = 0$. As we can appreciate, although the experimental points differ slightly from the theoretical curves, a good qualitative agreement is obtained. It has to be mentioned that the SLM was used in the maximal resolution of two pixels per spatial period of the grating. Since the properties of phase modulation of the SLM in high resolution are far from optimal, some differences between experimental points and the theoretical curve appear, mainly in the range $\theta \in [\pi, 2\pi)$ in Fig. 8(a). Such differences are more significant in the case $q = 1$ from where they are amplified by interference effects. The maximal violation of the Bell inequality occurs for $q = 1$ and there is no violation for $q = 0$ as expected. In Fig. 8(b) experimental and theoretical results corresponding to mixed states with density matrix defined in Eq. (7) are shown for $q = 1$, 2/3, 1/3, and 0. In this case the plot is shown not in the full range but in the zone of violation of the Bell inequality. The experimental results of the simulation are also in good agreement with the theory, within the experimental error. The lost of coherence of the state, when the parameter goes from the maximally entangled to the maximally mixed state, becomes evident in the transition from maximal violation to no violation.

7. CONCLUSIONS

We have implemented an optical setup to classically simulate Bell inequality violations. We have shown how a conventional optical processing architecture can be used to optically simulate a Bell-type experiment scenario. The simulation begins with the optical representation of the quantum state of two qubits as an image organized in four quarters according to the statement in Section 3. In this representation, pure and mixed states can be emu-

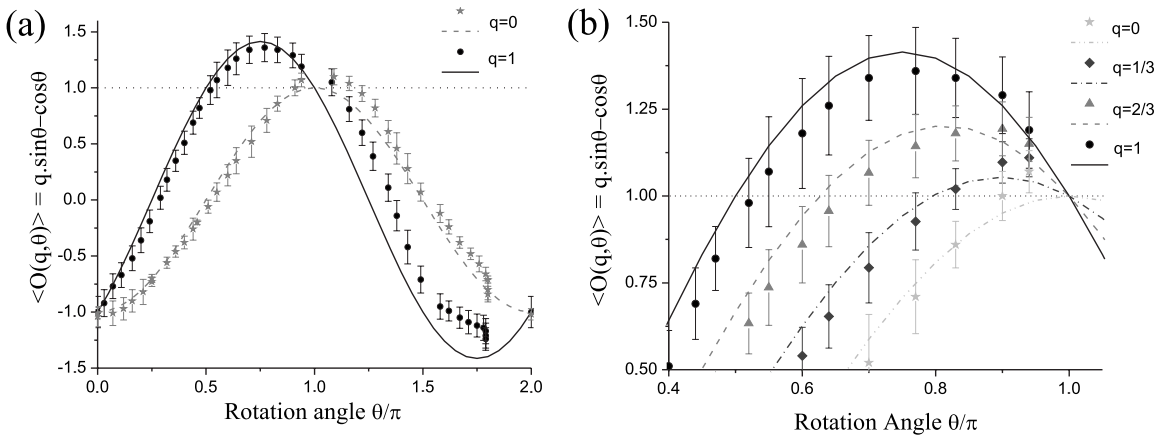

Fig. 8. Experimental results. (a) Theoretical predictions and experimental results of the simulation $\langle O\rangle$ versus θ plotted in the full range $\theta\in[0,2\pi)$ for the maximally entangled state $q=1$ and for the mixed state $q=0$. (b) Theoretical and experimental results of the simulations corresponding to mixed states with density matrix defined in Eq. (7) for $q=1$, 2/3, 1/3, and 0 in the Bell inequality violation domain.

lated. The encoded information is organized as a bipartite two level system. One part, conventionally called "Alice" has available dichotomic information related to the field distribution in the up-down direction of the scene. The second, "Bob" is associated with the orthogonal left-right direction. Quantum nonlocality arises from the assumption that the information available for one of the observers is unavailable for the other, and vice versa. Then, we process the input image with a 4*f* coherent optical processor with a phase grating in the Fourier plane. The optical processor is designed in order to ensure that the complex amplitude of the electromagnetic field is modified from the input to the output scene simulating a unitary evolution of the state. The simulated unitary evolution allows one to measure tensor products of local observables. Mean values of such quantities are experimentally evaluated from the intensity distribution of the field in the output image. We show that, depending on the encoded input state, correlated quantities calculated from the expected values of the observables violate a Clauser–Horne–Shimony–Holt Bell-type inequality.

In order to emphasize the role of interference effects in the Bell inequality violations, we test our setup in two different cases: in the first, the maximally entangled state $(|0\rangle_A\otimes|0\rangle_B+|1\rangle_A\otimes|1\rangle_B)/\sqrt{2}$ encoded in the input scene shows maximal violation; meanwhile, in the second, an incoherent superposition of $|0\rangle_A\otimes|0\rangle_B$ or $|1\rangle_A\otimes|1\rangle_B$ does not violate the Bell inequality mainly due to the absence of interference effects. Parametrical lost of coherence from maximally entangled to maximally mixed states has been simulated by means of an optical representation of a convex mixing of both types of states. In all cases, the experimental results of the simulations are in good agreement with the theoretical predictions based on quantum mechanics.

Summarizing, we have shown what we believe to be a novel classical optics simulation of the famous experiment of nonlocality testing proposed by Bell [12]. From a conceptual point of view we can say that, in principle, classical wave optics simulation of quantum information processing is completely equivalent to an analogical electronic computer which reproduces the interference effects that arise in real quantum systems. Since this kind of devices is decoherence free but nonscalable, they could be useful as testing tools for quantum information protocols in low dimensional Hilbert spaces. In addition, the knowledge and the optimization of these techniques could be adaptable to real quantum processes as those involving entangled photons, enhancing their potential applications to quantum information processing. Particularly, this simulation clearly illustrates how the mechanism of Bell inequality violations needs two resources: quantum entanglement and two-particle interference. It nicely demonstrates also that classical optics is a useful tool for a deeper understanding of some fundamental aspects of quantum mechanics. In the future, we plan to extend the results obtained in this work to the simulation of systems with multiparticle entanglement.

ACKNOWLEDGMENTS

The authors are grateful to Professor J. P. Paz and Professor Marcos Sareceno for the stimulating and fruitful discussions and comments. This research was financed by the projects Agencia Nacional de Promociones Cientificas y Técnicas ANPCYT PICT 25373, ANPCYT PICT 2284, Consejo Nacional de Investigaciones Científicas y Técnicas (CONICET) PIP 112, and UBACYT X118. S. Ledesma is a member of CONICET. M. A. Goldin is a CONICET fellow.

REFERENCES

1. N. J. Cerf, C. Adami, and P. G. Kwiat, "Optical simulation of quantum logic," Phys. Rev. A **57**, R1477–R1480 (1998).
2. R. J. C. Spreeuw, "A classical analogy of entanglement," Found. Phys. **28**, 361–374 (1998).
3. R. J. C. Spreeuw, Phys. Rev. A **63**, 062302 (2001).
4. N. Bhattacharya, H. B. van Linden vanden Heuvell, and R. J. C. Spreeuw, "Implementation of quantum search algorithm using classical Fourier optics," Phys. Rev. Lett. **88**, 137901 (2002).
5. G. Puentes, C. La Mela, S. Ledesma, C. Iemmi, J. P. Paz, and M. Saraceno, "Optical simulation of quantum algorithms using programmable liquid-crystal displays," Phys. Rev. A **69**, 042319 (2004).
6. D. Francisco, C. Iemmi, J. P. Paz, and S. Ledesma, "Optical

simulation of the quantum Hadamard operator," Opt. Commun. **268**, 340–345 (2006).
7. D. Francisco, C. Iemmi, J. P. Paz, and S. Ledesma, "Simulating a quantum walk with classical optics," Phys. Rev. A **74**, 052327 (2006).
8. D. Francisco and S. Ledesma, "Classical optics analogy of quantum teleportation," J. Opt. Soc. Am. B **25**, 383–390 (2008).
9. J. Fu, Z. Si, S. Tang, and J. Deng, "Classical simulation of quantum entanglement using optical transverse modes in multimode waveguides," Phys. Rev. A **70**, 042313 (2004).
10. K. F. Lee and J. E. Thomas, "Experimental simulation of two-particle quantum entanglement using classical fields," Phys. Rev. Lett. **88**, 097902 (2002).
11. A. Einstein, B. Podolsky, and N. Rosen, "Can quantum-mechanical description of physical reality be considered complete?" Phys. Rev. **47**, 777–780 (1935).
12. J. S. Bell, "On the Einstein–Podolsky–Rosen paradox," Physics (Long Island City, N.Y.) **1**, 195–200 (1964); reprinted in J. S. Bell, *Speakable and Unispeakable in Quantum Mechanics* (Cambridge U. Press, 1987).
13. A. Aspect, J. Dalibard, and G. Roger, "Experimental test of Bell's inequalities using time-varying analyzers," Phys. Rev. Lett. **49**, 1804–1807 (1982).
14. W. Tittel, J. Brendel, H. Zbinden, and N. Gisin, "Violation of Bell inequalities by photons more than 10 km apart," Phys. Rev. Lett. **81**, 3563–3566 (1998).
15. G. Weihs, T. Jennewein, C. Simon, H. Weinfurter, and A. Zeilinger, "Violation of Bell's inequality under strict Einstein locality conditions," Phys. Rev. Lett. **81**, 5039–5043 (1998).
16. A. Aspect, P. Grangier, and G. Roger, "Experimental tests of realistic local theories via Bell's theorem," Phys. Rev. Lett. **47**, 460–463 (1981).
17. A. Aspect, P. Grangier, and G. Roger, "Experimental realization of Einstein–Podolsky–Rosen–Bohm Gedankenexperiment: a new violation of Bell's inequalities," Phys. Rev. Lett. **49**, 91–94 (1982).
18. Z. Y. Ou and L. Mandel, "Violation of Bell's inequality and classical probability in a two-photon correlation experiment," Phys. Rev. Lett. **61**, 50–53 (1988).
19. P. G. Kwiat, K. Mattle, H. Weinfurter, A. Zeilinger, A. V. Sergienko, and Y. H. Shih, "New high-intensity source of polarization-entangled photons pair," Phys. Rev. Lett. **75**, 4337–4341 (1995).
20. D. M. Greenberger, M. Horne, and A. Zeilinger, "Going beyond Bell's theorem," in *Bell's Theorem, Quantum Theory and Conceptions of the Universe* (Kluwer Academic, 1989), pp. 73–76.
21. J. C. Howell, R. S. Bennink, S. J. Bentley, and R. W. Boyd, "Realization of The Einstein–Podolsky–Rosen paradox using momentum- and position-entangled photons from spontaneous parametric down conversion," Phys. Rev. Lett. **92**, 210403 (2004).
22. A. Beige, W. J. Munro, and P. L. Knight, "Bell's inequality test with entangled atoms," Phys. Rev. A **62**, 052102 (2000).
23. A. M. Souza, A. Magalhaes, J. Teles, E. R. deAzevedo, T. J. Bonagamba, I. S. Oliveira, and R. S. Sarthour, "NMR analog of Bell's inequalities violation test," New J. Phys. **10**, 033020 (2008).
24. M. Genovese, "Research on hidden variable theories: a review of recent progress," Phys. Rep. **413**, 319–396 (2005).
25. J. F. Clauser, M. A. Horne, A. Shimony, and R. A. Holt, "Proposed experiment to test local hidden-variable theories," Phys. Rev. Lett. **23**, 880–884 (1969).
26. N. Bohr, "Can quantum-mechanical description of physical reality be considered complete?" Phys. Rev. **48**, 696–702 (1935).
27. J. W. Goodman, *Introduction to Fourier Optics* (McGraw-Hill, 1996).
28. M. Nielsen and I. Chuang, *Quantum Information and Computation* (Cambridge U. Press, 2000).
29. A. Marquez, C. Iemmi, I. Moreno, J. A. Davis, J. Campos, and M. J. Yzuel, "Quantitative prediction of the modulation behavior of twisted nematic liquid crystal displays based on a simple physical model," Opt. Eng. (Bellingham) **40**, 2558–2564 (2001).